Activation Energy Spectra: Insights into Transport Limitations of Organic Semiconductors and Photovoltaic Cells

*Ziqi Liang, Alexandre M. Nardes, Jao van de Lagemaat, and Brian A. Gregg**

Some mechanisms of charge transport in organic semiconductors and organic photovoltaic (OPV) cells can be distinguished by their predicted change in activation energy for the current, E_a, versus applied field, F. E_a versus F is measured first in pure films of commercially available regioregular poly(3-hexylthiophene) (P3HT) and in the same P3HT treated to reduce its charged defect density. The former shows a Poole–Frenkel (PF)-like decrease in E_a at low F, which then plateaus at higher F. The low defect material does not exhibit PF behavior and E_a remains approximately constant. Upon addition of [6,6]-phenyl-C_{61}-butyric acid methyl ester (PCBM), however, both materials show a large increase in E_a and exhibit PF-like behavior over the entire field range. These results are explained with a previously proposed model of transport that considers both the localized random disorder in the energy levels and the long-range electrostatic fluctuations resulting from charged defects. Activation energy spectra in working OPV cells show that the current is injection-limited over most of the voltage range but becomes transport-limited, with a large peak in E_a, near the open circuit photovoltage. This causes a decrease in fill factor, which may be a general limitation in such solar cells.

1. Introduction

Organic photovoltaic (OPV) cells and the semiconductors they are made from have been studied intensively in recent years.[1] Bulk heterojunctions (BHJs) consisting of a blend of a π-conjugated polymer, archetypically regioregular poly(3-hexylthiophene) (P3HT) and an acceptor such as [6,6]-phenyl-C_{61}-butyric acid methyl ester (PCBM) are currently the most efficient type of OPV cell, reaching certified efficiencies of 6–8%.[2] Much remains to be learned, however, about transport and carrier recombination, amongst other topics, even in the much-studied P3HT:PCBM BHJ cells. Transport in such polymers is the subject of much ongoing research.[3–5] Numerous models have been proposed but there is still no general agreement about which is most appropriate. Many of the models neglect the effect of charged defects in the semiconductor. We previously estimated that if the total charge density were significantly below $N_{cd} \approx 10^{17}$ cm^{-3}, the electrostatic effects of these charges on transport could reasonably be neglected.[6] However, we also estimated that in P3HT, $N_{cd} > 10^{18}$ cm^{-3},[7] which should strongly affect transport. Unfortunately, there are no reported measurements of N_{cd} to our knowledge, but the free hole (polaron) density, p_f, in a p-type polymer provides a useful lower limit to it.

The change in activation energy, E_a, for the current as a function of applied electric field, F, provides a useful tool that can distinguish between some of the different transport mechanisms. Here, we compare two types of P3HT with different charge densities. The commercially available form of P3HT (Rieke Metals) has a free hole density of $p_f = 5.3 \times 10^{16}$ cm^{-3}[5,7] comparable to similar polymers.[8] We earlier developed several chemical treatments of P3HT that reduce its defect density while simultaneously increasing the carrier mobility, the exciton diffusion length, and the stability of the polymer against photo-oxidation.[7,9] For comparison to the commercial P3HT, we employ here the lowest defect density material we have: lithium aluminum hydride treated P3HT (LAH-P3HT), which has $p_f = 3.9 \times 10^{15}$ cm^{-3}. The E_a versus F properties of these two P3HTs are compared in pure bulk films, in films with added PCBM, and in working OPV cells. The results reveal several aspects of transport in these materials and what limits it under different circumstances.

2. Results and Discussion

2.1. Bulk Transport in the Pure Polymers

In order to study E_a versus F in nearly identical materials with different charge densities, we compare P3HT ($p_f = 5.3 \times 10^{16}$ cm^{-3}) to LAH-P3HT ($p_f = 3.9 \times 10^{15}$ cm^{-3}).[7,9] Although N_{cd} is not known in these polymers, we can plausibly assume that since the LAH treatment decreased p_f, it also decreased N_{cd}. The activation energies of the dark currents versus F were first measured in films of the two types of P3HT on interdigitated electrodes (IDEs). The platinum electrodes of the IDE are spaced 10 μm apart. This large spacing ensures that the applied potential drops almost linearly across the bulk

Dr. Z. Liang, Dr. A. M. Nardes, Dr. J. van de Lagemaat, Dr. B. A. Gregg
National Renewable Energy Laboratory
1617 Cole Boulevard, Golden, CO 80401, USA
E-mail: brian.gregg@nrel.gov

DOI: 10.1002/adfm.201102813

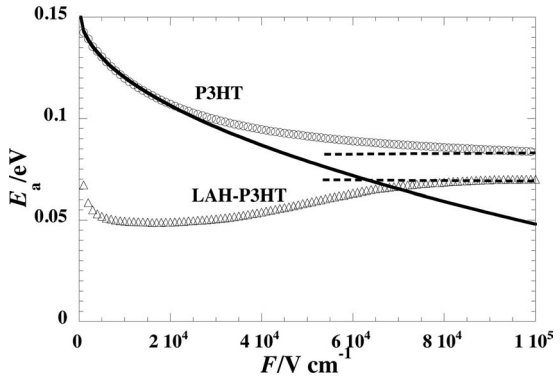

Figure 1. Activation energies for dark currents vs. field for as-purchased P3HT and for the low-defect LAH-P3HT. The data are from films on interdigitated electrodes and represent bulk-transport-limited currents. The solid line is a fit of Equation 1 to the P3HT data up to $F = 2 \times 10^4$ V cm^{-1}.

producing a uniform electric field and that the dark currents are almost entirely bulk-transport-limited.[10] These currents are in the Ohmic or Poole-Frenkel regime; they are not space-charge-limited. Representative raw data are shown in the Supporting Information, Figure S2. The results in **Figure 1** reveal a qualitative difference between the two types of P3HT. The low doped material, LAH-P3HT shows a slight decrease in E_a at low field, which then slowly increases back to about its starting value of ≈70 meV at 10^5 V cm^{-1}. On the other hand, the higher doped material, P3HT, shows a rapid decline in E_a from ≈150 meV to a plateau of ≈80 meV at higher field.

2.2. Model

As mentioned, there are many models of transport in organic semiconductors. Most of them emphasize the effects of random disorder in the localized energy levels, but they do not generally take into account the charged defect density, N_{cd}, in the material and its associated long-range electrostatic perturbation of these energy levels. To discuss our data, we employ a simple model introduced previously that accounts semiquantitatively for both the charged defect density and the energetic disorder.[6] The model presented in **Figure 2**a shows the site-to-site energetic disorder in the polymer film perturbed (and thus correlated) by the long range Coulomb potentials resulting from charges in the semiconductor. The $E_{a,PF}$ due to the Coulomb potential decreases with the square root of the field in the Poole–Frenkel (PF) model (Equation 1 and Figure 2b):

$$E_{a,PF} = E_{a0} - a(q^3/\pi\varepsilon_0\varepsilon)^{1/2} F^{1/2} \quad (1)$$

where E_{a0} is the zero-field E_a, q is the electronic charge, ε_0 is the permittivity of free space, ε is the dielectric constant (assumed to be 4), and a is often near 0.5. The PF model is a much simplified approximation to the electrostatic landscape in a real material and it is strictly valid only for 1D systems. Still, it often gives a surprisingly accurate estimation of electric field effects in doped low dielectric materials.[10,11]

In contrast to $E_{a,PF}$ in Figure 2, $E_{a,D}$ due to the static energy disorder should remain more or less constant with field.[3] The

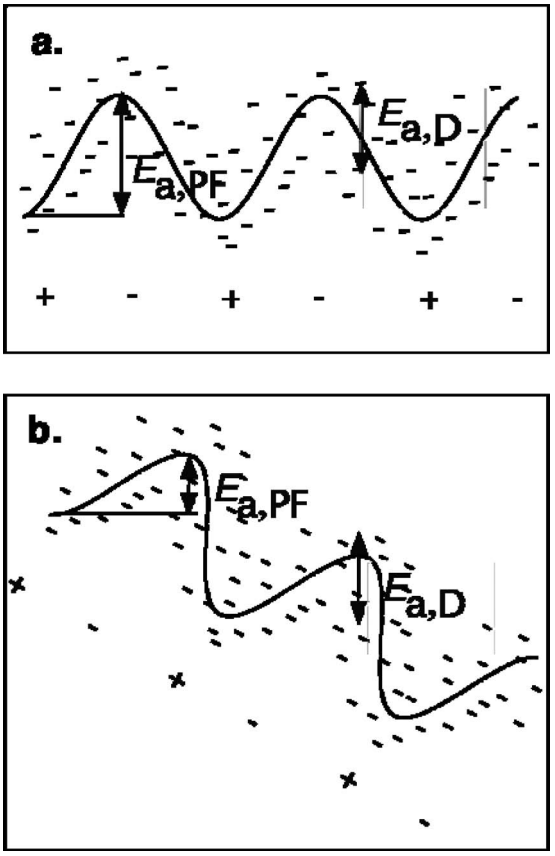

Figure 2. Model showing the randomly disordered local energy levels of a polymer perturbed by the long range Coulomb fields resulting from charged defects. The PF and the static disorder activation energies are shown. a) Zero field and b) under applied bias.

fundamental distinction is that an applied field will significantly perturb long-range Coulomb barriers, but it will not greatly influence the relative energetics between two neighboring hopping sites. Thus, substantial changes in E_a with F are likely indicative of long-range electrostatic fluctuations. The P3HT data in Figure 1 are fit to Equation 1 up to $F = 2 \times 10^4$ V cm^{-1} with $a = 0.87$. Attempts to apply the equation at higher fields led to increasingly poorer fits.

The model of Figure 2 makes two predictions, both of which seem to be supported by the data in Figure 1. One is that the transport-limiting mechanism may change from PF to disorder-limited in a given material as the field is increased (see Figure 1, P3HT curve, and compare Figure 2a to b). This occurs because $E_{a,PF}$ decreases with field while $E_{a,D}$ remains more or less constant. The second, discussed previously,[6] is that the transport mechanism can change from non-PF to PF as the charge density increases in a given material (compare LAH-P3HT to P3HT in Figure 1). This should occur because at low values of N_{cd}, charge carriers can often go around electrostatic barriers rather than over them. The experiments reported here were designed in part to test these two predictions.

The lower doped material in Figure 1, LAH-P3HT, shows slight changes in E_a with F, which are not fully understood, but there are no significant trends. According to the model, this results from its low charged defect density leading to $E_{a,PF} < E_{a,D}$

even at zero field. In this case, the measured E_a can be associated with the disorder parameter in LAH-P3HT, $\Delta \approx 70$ meV. In the more highly doped material, the plateau in E_a at higher field provides the estimate that in P3HT, $\Delta \approx 80$ meV. The static disorder in the two cases is similar, suggesting that the two polymers are electronically quite comparable to each other and differ primarily in p_f and N_{cd}.

2.3. Bulk Transport in the Polymer:PCBM Blends

Similar experiments with PCBM, the most common acceptor species in BHJ OPV cells, blended into the two P3HTs (0.8:1.0 by weight) show much higher values of E_a under transport-limited conditions, **Figure 3**. In the blend films both types of P3HT show PF-like behavior over the entire range of field. The dark values are fit well to Equation 1, except very near zero-field, with $a = 0.47$ and 0.63 for the P3HT and LAH-P3HT films, respectively. In the context of the model, both the increase in E_a, and the PF-like behavior at higher fields relative to the pure polymer case, are consistent with a substantial increase in charge density caused by adding PCBM. Illumination of the films decreases E_a considerably, consistent with an increase in free carrier density that more efficiently screens the fixed charges and fills the deeper levels, or in other words, the quasi-Fermi levels shift toward the extended states in which conduction occurs. These values also are well fit by Equation 1, except near zero-field, with $a \approx 0.37$. The results near zero-field may no longer be in the bulk transport limited regime due to electrode-specific effects.

2.4. Transport in BHJ OPV Cells

Finally, E_a spectra were measured in complete BHJ OPV cells made from each polymer (**Figure 4**) with a configuration of indium tin oxide (ITO)/poly(3,4-ethylenedioxythiophene):poly(styrenesulfonate) (PEDOT:PSS)/P3HT:PCBM/LiF/Al (see Experimental Section). Representative raw data are shown in Figure S1 (Supporting Information). A cell is a much different environment than the interdigitated electrodes employed for the earlier experiments, which measured only bulk transport properties. In a cell, the two electrodes have different work functions creating an internal

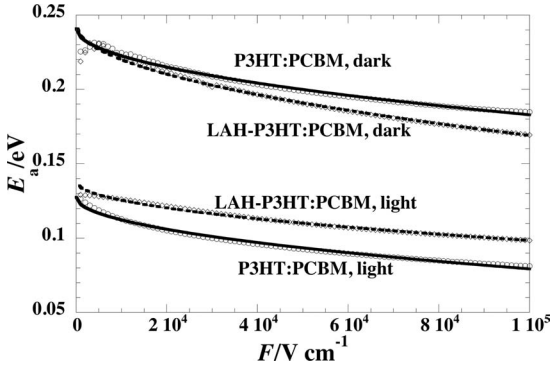

Figure 3. Activation energies for currents vs. field on IDEs for both types of P3HT after addition of PCBM. The values in the dark and under 1 sun illumination are shown. The solid lines are fits to Equation 1.

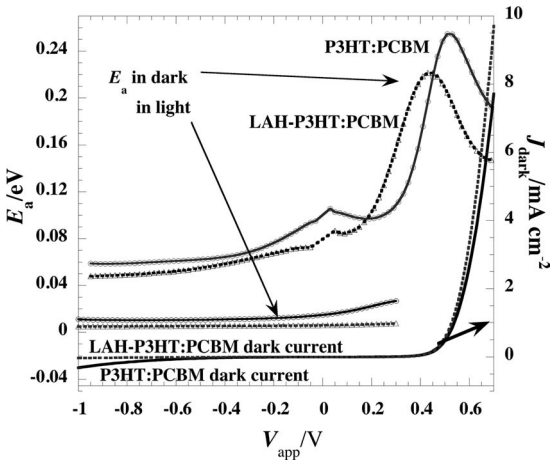

Figure 4. Activation energy spectra of BHJ OPV cells for both types of P3HT with PCBM in the dark and under 1 sun illumination. The dark current–voltage curves of the two cells are shown relative to the right hand axis.

electric field, and the electrodes are spaced only ≈150 nm apart. The measured E_a in the dark will be that of whichever process limits the current: either injection or bulk transport.

The two dark current-voltage curves (Figure 4, right hand axis) are quite similar but the LAH-P3HT cell shows better diode behavior: lower reverse current and higher forward current at the voltage extremes. This may account for its slightly better PV properties. The diode turn-on voltage for both cells is ≈0.5 V. This voltage should be similar to the potential of zero field in the cell, at which the applied potential cancels the cell's built-in potential, $V_{app} = -V_{bi}$. These E_a values may thus be compared to the $F = 0$ values in Figure 3.

The most remarkable result in Figure 4 is the appearance of large peaks in E_a near the zero internal field point. The E_a decreases rapidly on both sides of these peaks, although we cannot measure accurately very far into forward bias. The magnitude of the two peaks is quite similar to that of the transport-limited results at zero field in Figure 3. Under reverse bias, E_a drops much more quickly in the cell than in the IDEs and plateaus at a level far below that seen in Figure 3 at similarly high field. (To compare the two figures: the –1 V position in Figure 4 corresponds to $F \approx 10^5$ V cm^{-1} in Figure 3.) We interpret this as evidence that the dark currents are injection-limited (a common assumption)[12] up to near the point of zero internal field. At this point the currents are so low that they are no longer injection-limited and become transport-limited, with a consequent large rise in E_a. Thus we interpret the peaks in E_a versus V_{app} as being due to a transition from injection limited currents over most of the voltage range to transport-limited currents near V_{bi}. The small shoulders near $V_{app} = 0$ may herald the beginning of transport limitation although still under a relatively high internal electric field.

Under illumination, E_a in the cells drops significantly. We cannot measure E_a by our procedure near $V_{app} = -V_{bi}$ because of the temperature dependence of the open circuit photovoltage, V_{oc}. However, if we assume that the low currents that occur near V_{oc} will be transport limited, as they are in the dark, then the E_a values should be similar to those of the illuminated zero-field values in Figure 3. This large increase in E_a (up to

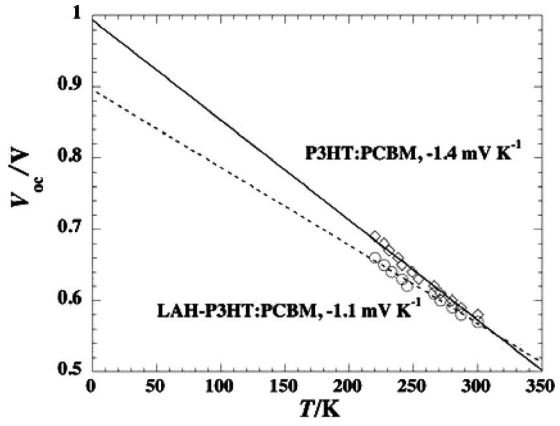

Figure 5. Temperature dependence of V_{oc} extrapolated to $T = 0$ K.

≈125 meV) near V_{oc} will cause a decrease in fill factor, *FF*, and thus in the conversion efficiency of the cell. From our analysis it seems that this might be a general phenomenon limiting OPV cells that has not been identified before in this and other BHJ systems.

Under illumination, the measured average photovoltaic properties of the P3HT:PCBM and LAH-P3HT:PCBM cells, respectively, were: V_{oc} = 584 and 573 meV; short circuit photocurrent density, J_{sc} = 7.4 and 7.6 mA cm^{-2}; *FF* = 60 and 63; and power conversion efficiency, PCE = 2.5 and 2.7%.

2.5. Temperature Dependence of V_{oc}

The photovoltage shows a linear dependence on temperature (**Figure 5**). When extrapolated to a temperature $T = 0$ K, this leads to the theoretical maximum V_{oc}:[13]

$$V_{oc,max} = (1/q)(E_{lumo} - E_{homo} - \Delta) \quad (2)$$

where E_{lumo} and E_{homo} refer to the energies of the lowest unoccupied molecular orbital of PCBM and the highest occupied molecular orbital of P3HT, respectively. The ≈100 meV decrease in $V_{oc,max}$ in the LAH-treated material suggests that the valence band edge of LAH-P3HT is ≈100 meV above that of untreated P3HT. Even with this deficiency, though, the LAH-P3HT makes a more efficient OPV cell at room temperature, partly because of its lower E_a for transport.

3. Conclusions

We describe several unusual transitions in this paper. A transition from Poole-Frenkel to non-PF behavior with increasing field (Figure 1, P3HT); a transition from non-PF to PF behavior with increasing charged defect density (Figure 1, compare LAH-P3HT to P3HT); and a transition from injection-limited current to transport-limited current near the zero internal field point in OPV cells (Figure 4). The first two transitions are predicted from a simple model of transport (Figure 2 and ref. [6]), while the third may be reported here for the first time. Measuring activation energy spectra in model systems and devices is a powerful tool for characterizing transport in organic semiconductors. Our results point to a potentially fundamental transport limitation in OPV cells near V_{oc} and provide support for a model of transport that combines the influence of long-range Coulomb forces with short-range energetic disorder.

4. Experimental Section

Materials: P3HT and PCBM were obtained from Rieke Metals, Inc. (Item 4002-EE, 90–93% regioregularity) and Nano-C, Inc. (Item nano-CPCBM-BF), respectively, and used as received. All other chemical reagents and solvents were obtained from Aldrich and used without further purification.

Sample Preparations: Preparation of P3HT and P3HT:PCBM blend film samples was carried out in a N_2 atmosphere glovebox. P3HT (15 mg mL^{-1}) and P3HT:PCBM blend (1.0:0.8 by weight, 18 mg mL^{-1} in total concentration) were dissolved in anhydrous chlorobenzene with heating and stirring overnight. Films were made by spin-coating with a KW-4A spin-coater (Chemat Technology) on Pt interdigitated electrodes (IDEs, AbTech Scientific) with an electrode spacing of 10 μm to yield a thickness approximately equal to the electrode height of ≈110 nm. All the films were then annealed at 130 °C for 15 min on a hotplate in the glovebox before the characterization and measurement. Film thickness was measured on an Alpha-step profilometer (Veeco Dektak 8 Advanced Development Profiler). For the fabrication of BHJ cells, patterned indium tin oxide (ITO) substrates (12 Ω □$^{-1}$; Thin Film Devices, Inc.) were cleaned ultrasonically by successive sonications in solvent baths of detergent, distilled water, acetone, and isopropyl alcohol. After drying with a stream of N_2, the substrates were exposed to UV-ozone (UVO Cleaner 42, Jelight Company, Inc.) at ≈28 mW cm^{-2} for 5 min. The PEDOT-PSS (Clevios) layer of ≈30 nm was spin-coated onto the ITO at 4000 rpm for 30 s and then baked on a hotplate at 120 °C for 60 min. Then the PEDOT-coated substrates were immediately transferred to a N_2-filled glovebox for making the active layer. A blend of P3HT:PCBM (1:0.8 by weight) in anhydrous chlorobenzene with a total concentration of 18 mg mL^{-1} was spin-coated onto the PEDOT:PSS-coated ITO glass slides at 400 to 600 rpm for 60 s, yielding the ≈150-nm thick active layer. The samples were then loaded into a glovebox-integrated deposition chamber (Angstrom Engineering) and pumped down to a pressure of $<2 \times 10^{-7}$ Torr. Back electrodes of LiF (0.6 nm) and Al (100 nm) were deposited sequentially by thermal evaporation through a shadow mask at a rate of 0.1 Å s^{-1} and 2 Å s^{-1}, respectively. The shadow mask was used to define 6 pixels per substrate, where the active area was defined by the overlap of ITO anode and Al cathode as 0.11 cm^2.

Electrical Measurements: Current–voltage (*I–V*) curves of P3HT and P3HT:PCBM blend on IDE substrates were acquired on a Keithley 236 Source Measure Unit (SMU). For BHJ cells based on P3HT:PCBM blends, the current density–voltage (*J–V*) characteristics were measured with a Keithley 236 SMU while illuminated with a home-made solar simulator at 100 mW cm^{-2}. Solar-simulator illumination intensity was measured using a standard silicon photodiode (Hamamatsu S1787-04) with a protective KG filter calibrated by NREL's Measurement and Characterization group. Note that all data values from the *J–V* curves are an average of all six pixels on a single substrate.

Activation Energy: Temperature-dependent electrical measurements (*J–V–T*) were performed in a Janis Research VPF-475 cryostat coupled with a temperature controller (Lakeshore Model 330) in the range of 110 to 310 K. Electric field dependence was obtained from *J–V–T* curves by sweeping the voltage bias from −1 to 1 V at a step size of 10 mV on the BHJ cells or from −100 to 100 V at a step size of 1 V on the IDE samples. The activation energy, E_a, was obtained at each applied voltage from the slope of the Arrhenius plot of ln*I* versus 1/*kT*, where *k* is Boltzmann's constant and *T* is absolute temperature.

Supporting Information

Supporting Information is available from the Wiley Online Library or from the author.

Acknowledgements

The authors are grateful for stimulating discussions with Jian Li and Sean Shaheen. This work was funded by the U.S. Department of Energy, Office of Science, Basic Energy Science, Division of Chemical Sciences, Geosciences and Biosciences, under Contract No. DE-AC36-08GO28308 to NREL.

Received: November 21, 2011
Published online: December 29, 2011

[1] a) T. M. Clarke, J. R. Durrant, *Chem. Rev.* **2010**, *110*, 6736; b) C. Deibel, V. Dyakonov, *Rep. Prog. Phys.* **2010**, *73*, 096401; c) A. Facchetti, *Chem. Mater.* **2011**, *23*, 733; d) A. W. Hains, Z. Liang, M. A. Woodhouse, B. A. Gregg, *Chem. Rev.* **2010**, *110*, 6689; e) Y. Liang, L. Yu, *Acc. Chem. Res.* **2010**, *43*, 1227; f) B. Walker, C. Kim, T.-Q. Nguyen, *Chem. Mater.* **2011**, *23*, 470; g) N. R. Armstrong, P. A. Veneman, E. Ratcliff, D. Placencia, M. Brumbach, *Acc. Chem. Res.* **2009**, *42*, 1748; h) G. Dennler, M. C. Scharber, C. J. Brabec, *Adv. Mater.* **2009**, *21*, 1; i) B. Kippelen, J.-L. Brédas, *Energy Environ. Sci.* **2009**, *2*, 251.

[2] a) H.-Y. Chen, J. Hou, S. Zhang, Y. Liang, G. Yang, Y. Yang, L. Yu, Y. Wu, G. Li, *Nat. Photonics* **2009**, *3*, 649; b) M. A. Green, K. Emery, Y. Hishikawa, W. Warta, *Prog. Photovolt: Res. Appl.* **2011**, *19*, 84.

[3] H. Bässler, *Phys. Stat. Solidi* **1993**, *175*, 15.

[4] a) T. Kreouzis, D. Poplavskyy, S. M. Tuladhar, M. Campoy-Quiles, J. Nelson, A. J. Campbell, D. D. C. Bradley, *Phys. Rev. B* **2006**, *73*, 235201; b) V. Coropceanu, J. Cornil, D. A. da Silvo Filho, Y. Olivier, R. Silbey, J.-L. Brédas, *Chem. Rev.* **2007**, *107*, 926; c) G. Dicker, M. P. de Haas, J. M. Warman, D. M. de Leeuw, L. D. A. Siebbeles, *J. Phys. Chem. B* **2004**, *108*, 17818; d) S. V. Novikov, *Phys. Stat. Sol.* **2003**, *236*, 119; e) P. W. M. Blom, V. D. Mihailetchi, L. J. A. Koster, D. E. Markov, *Adv. Mater.* **2007**, *19*, 1551; f) S. Günes, H. Neugebauer, N. S. Sariciftci, *Chem. Rev.* **2007**, *107*, 1324; g) V. I. Arkhipov, P. Heremans, E. V. Emilianova, H. Bässler, *Phys. Rev. B* **2005**, *71*, 045214; h) S. V. Novikov, D. H. Dunlap, V. M. Kenkre, P. E. Parris, A. V. Vannikov, *Phys. Rev. Lett.* **1998**, *81*, 4472; i) S. V. Rakhmanova, E. M. Conwell, *Appl. Phys. Lett.* **2000**, *76*, 3822; j) E. A. Katz, D. Faiman, S. M. Tuladhar, J. M. Kroon, M. M. Wienk, T. Fromherz, F. Padinger, C. J. Brabec, N. S. Sariciftci, *J. Appl. Phys.* **2001**, *90*, 5343; k) K. Maturová, S. S. v. Bavel, M. M. Wienk, R. A. J. Janssen, M. Kemerink, *Adv. Funct. Mater.* **2011**, *21*, 261.

[5] A. J. Morfa, A. M. Nardes, S. E. Shaheen, N. Kopidakis, J. v. d. Lagemaat, *Adv. Funct. Mater.* **2011**, *21*, 2580.

[6] B. A. Gregg, *J. Phys. Chem. C* **2009**, *113*, 5899.

[7] Z. Liang, A. Nardes, D. Wang, J. J. Berry, B. A. Gregg, *Chem. Mater.* **2009**, *21*, 4914.

[8] a) G. Garcia-Belmonte, A. Munar, A. M. Barea, J. Bisquert, I. Ugarte, R. Pacios, *Org. Electron.* **2008**, *9*, 847; b) P. P Boix, M. M. Wienk, R. A. J. Janssen, G. Garcia-Belmonte, *J. Phys. Chem. C* **2011**, *115*, 15075; c) C. G. Shuttle, R. Hamilton, J. Nelson, B. C. O'Regan, J. R. Durrant, *Adv. Funct. Mater.* **2010**, *20*, 698; d) C. P. Jarrett, R. H. Friend, A. R. Brown, D. M. de Leeuw, *J. Appl. Phys.* **1995**, *77*, 6289.

[9] Z. Liang, M. Reese, B. A. Gregg, *ACS Appl. Mater. Interfaces* **2011**, *3*, 2042.

[10] S.-G. Chen, P. Stradins, B. A. Gregg, *J. Phys. Chem. B* **2005**, *109*, 13451.

[11] J. G. Simmons, *Phys. Rev.* **1967**, *155*, 657.

[12] a) F. Neuman, Y. A. Genenko, C. Melzer, H. von Seggern, *J. Appl. Phys.* **2006**, *100*, 084511; b) J. C. Scott, *J. Vac. Sci. Technol. A* **2003**, *21*, 521.

[13] S. R. Cowan, A. Roy, A. J. Heeger, *Phys. Rev. B* **2010**, *82*, 245207.